

**Processes regulating pCO₂
in the surface waters
of the central eastern
Gotland Sea: a model
study***

doi:10.5697/oc.53-2.745
OCEANOLOGIA, 53 (3), 2011.
pp. 745–770.

© Copyright by
Polish Academy of Sciences,
Institute of Oceanology,
2011.

KEYWORDS

Biogeochemical modelling
Baltic Sea
Non-Redfield stoichiometry
Nitrogen fixation

IVAN KUZNETSOV^{1,*}
THOMAS NEUMANN¹
BERND SCHNEIDER¹
EVGENIY YAKUSHEV²

¹ Leibniz Institute for Baltic Sea Research,
Seestrasse 15, Rostock-Warnemünde 18119, Germany;

e-mail: ivan.kuznetsov@smhi.se

*corresponding author

² Norwegian Institute for Water Research,
PO Box 333, Blindern, Oslo 3, Norway

Received 22 March 2011, revised 18 July 2011, accepted 2 August 2011.

Abstract

This work presents a one-dimensional simulation of the seasonal changes in CO₂ partial pressure (pCO₂). The results of the model were constrained using data from observations, which improved the model's ability to estimate nitrogen fixation in the central Baltic Sea and allowed the impact of nitrogen fixation on the ecological state of the Baltic Sea to be studied. The model used here is the public

* The German section of the Baltic Monitoring Programme (COMBINE) in the Baltic Sea is conducted by the IOW on behalf of the Bundesamt für Seeschifffahrt und Hydrographie (BSH), financed by the Bundesministerium für Verkehr, Bau- und Wohnungswesen (BMCBW). This work was funded by DFG grant: NE G17/3-1 and the European Community's Seventh Framework Programme (FP/2007–2013) under grant agreement 217246 made with the joint Baltic Sea research and development programme BONUS (ECOSUPPORT).

The complete text of the paper is available at <http://www.iopan.gda.pl/oceanologia/>

domain water-column model GOTM (General Ocean Turbulence Model), which in this study was coupled with a modified Baltic Sea ecosystem model, ERGOM (The Baltic Sea Research Institute's ecosystem model). To estimate nitrogen fixation rates in the Gotland Sea, the ERGOM model was modified by including an additional cyanobacteria group able to fix nitrogen from March to June. Furthermore, the model was extended by a simple CO_2 cycle. Variable C:P and N:P ratios, controlled by phosphate concentrations in ambient water, were used to represent cyanobacteria, detritus and sediment detritus. This approach improved the model's ability to reproduce sea-surface phosphate and pCO_2 dynamics. The resulting nitrogen fixation rates in 2005 for the two simulations, with and without the additional cyanobacteria group, were 259 and $278 \text{ mmol N m}^{-2} \text{ year}^{-1}$ respectively.

1. Introduction

The Baltic Sea is a small sea on a global scale, but at the same time one of the largest bodies of brackish water in the world. With an average depth of 53 m , it contains $21\,547 \text{ km}^3$ of water, and every year rivers contribute 2% to this volume (HELCOM 2003). The narrow and shallow Danish Straits (Kattegat region, Figure 1) connect the Baltic Sea with the North Sea and limit the exchange of water between the Baltic Sea and the world's oceans. Because of this strongly limited water exchange with the North Sea, the residence time of Baltic Sea waters can be as long as several decades (BACC Author Team 2008). Surface salinity varies from 20 PSU in the Kattegat

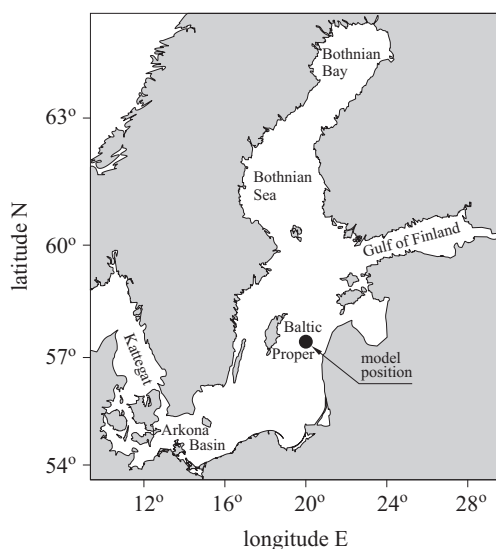


Figure 1. The Baltic Sea. The area of the model is indicated by a black dot (the deepest area of the eastern Gotland Sea)

to 1–2 PSU in the Bothnian Bay. The vertical structure of the central Baltic Sea is characterized by permanent salinity and density stratification, the halocline, which limits the vertical exchange of water. The area of our investigation was the Gotland Sea, one of the Baltic Sea's sub-basins (Figure 1).

Although the Baltic Sea is one of the most intensively investigated seas, not all of its biogeochemical processes are clearly understood and the results of different research efforts have frequently been controversial. One of the most important processes in the ecosystem of the Baltic Sea is nitrogen fixation, which plays a significant role in the balance of the marine nutrient budget. The Baltic Sea is one of the few brackish water areas in the world where nitrogen-fixing cyanobacteria, some of which are toxic, are an important component of the phytoplankton (Howarth et al. 1988).

Estimates of N₂ fixation rates have been obtained by different methods. Model studies of N₂ fixation rates were carried out by Savchuk & Wulff (1999), Leinweber (2002) and Neumann & Schernewski (2008). In addition, different measurement-based methods, such as those for nitrogen, phosphate and CO₂ budgets (Rahm et al. 2000, Larsson et al. 2001, Schneider et al. 2003, 2009a), N¹⁵ isotope tracer techniques (Wasmund et al. 2001) and ocean colour satellite data (Kahru et al. 2007) have been used to evaluate nitrogen fixation rates. However, these different estimates give N₂ fixation rates varying from 10 to 318 mmol m⁻² year⁻¹.

Mathematical modelling of marine ecosystems is an effective way of improving both our understanding of biogeochemical processes and the estimation of marine ecological states. An important step in this type of modelling work is the verification of ecosystem models. The carbon cycle unites most components of the biogeochemical processes that characterize a marine ecosystem, but at the same time carbon is not the limiting factor for processes such as primary production. Although most ecological models are not calibrated to CO₂, the addition of a carbon cycle to a biogeochemical model can contribute to its verification. Unique CO₂ partial pressure (pCO₂) data, measured from the ferries that run between Helsinki and Lübeck (Schneider et al. 2006, 2009a), can be used to validate the results of such models.

Leinweber (2002) attempted to simulate the seasonal changes of pCO₂ in the Baltic Sea; however, this was achieved only by unrealistic assumptions such as PO₄ concentrations twice as large as the observed values. A more successful attempt was undertaken by Omstedt et al. (2009). With a physical-biogeochemical box model these authors reproduced the long-term dynamics of the carbon cycle as well as seasonal variations of pH and pCO₂.

The aim of this study was to simulate seasonal changes in the CO₂ system of the Baltic Sea and to validate modelling results with observational data. This approach resulted in an improvement of the model's ability to estimate nitrogen fixation rates and primary production in the central Baltic Sea, and to study the impact of nitrogen fixation on the development of the ecological state of the sea.

2. Methodology

The model used in this work is the public domain water-column model GOTM (General Ocean Turbulence Model, see www.gotm.net; Burchard et al. (2006)), which was coupled with a modified Baltic Sea ecosystem model ERGOM (Neumann et al. 2002). GOTM is based on the Reynolds-averaged Navier-Stokes equations in a rotating reference frame, as well as on the Reynolds-averaged versions of the transport equations of temperature and salinity. In the GOTM, specific emphasis has been placed on the implementation of two-equation statistical turbulence closure models with algebraic second-moment closures (for an overview, see Burchard (2002), Umlauf & Burchard (2003) and Umlauf & Burchard (2005)). The biogeochemical ERGOM model is coupled to the physical model as an Eulerian-type model in which all state variables, dissolved elements (O₂, NH₄, PO₄, etc.) and particles (zooplankton, phytoplankton, etc.), are expressed as concentrations. A detailed description of the coupling of the GOTM and ERGOM models can be found in Burchard et al. (2006).

The basic structure of the biogeochemical model is explained in Figure 2. It consists of 18 state variables, including the nutrient state variables of dissolved ammonium, nitrate and phosphate. Primary production is provided by four functional phytoplankton groups: diatoms, flagellates and two groups of cyanobacteria. Diatoms are large cells that grow rapidly in nutrient-rich conditions. Flagellates are smaller cells with an advantage at lower nutrient concentrations during summer conditions. Since cyanobacteria are able to fix and utilize atmospheric elemental nitrogen, the model assumes that phosphate is the only limiting nutrient for this group. In addition, owing to their ability to fix nitrogen, cyanobacteria are a nitrogen source for the ecosystem. A dynamically developing bulk zooplankton variable provides grazing pressure on the phytoplankton. Dead particles are considered as a detritus state variable. The detritus is mineralized into dissolved ammonium, phosphate and total CO₂ during the sedimentation process. A certain amount of the detritus reaches the bottom, where it accumulates in the sedimentary detritus. In the model, the development of oxygen is coupled to the biogeochemical processes via stoichiometric ratios (Table 7, see Appendix page 770), with the oxygen concentration controlling

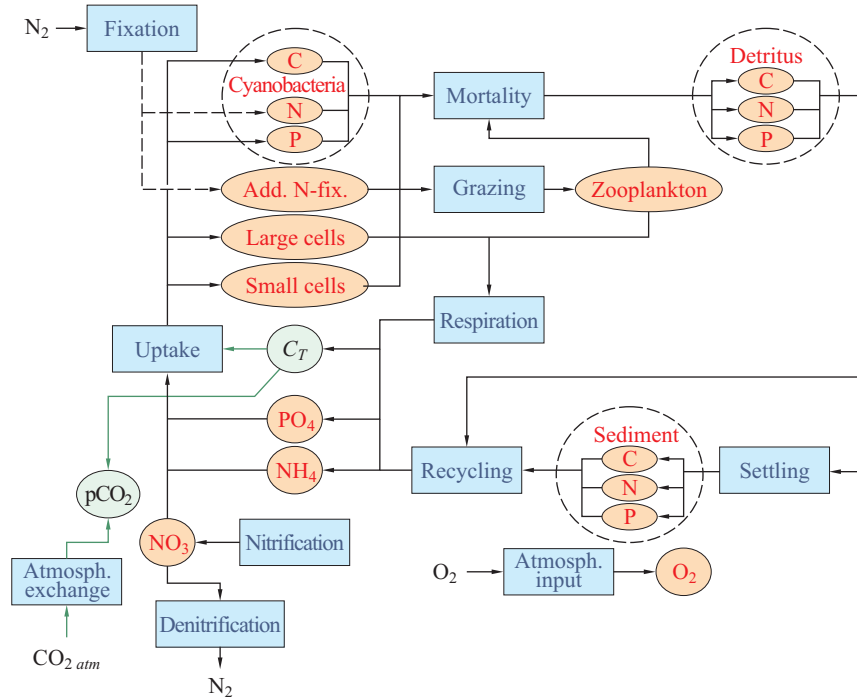


Figure 2. Structure of the biogeochemical model, which includes C, N and P in cyanobacteria, diatoms (large cells), flagellates (small cells), an additional cyanobacteria group (Add.N-Fix.) and zooplankton; C, N and P in detritus; C, N and P in sediment detritus as well as ammonium (NH₄), nitrate (NO₃), phosphate (PO₄), carbon (C_T) and oxygen (O₂). The orange and green ovals are model state variables; the blue rectangles are model processes. (For an interpretation of the references to colour in this figure caption, the reader is referred to the web version of the article)

processes such as denitrification, nitrification and sulphate reduction. All the variables of the model are presented in Table 1. The equations of the model can be found in the Appendix. ERGOM has been successfully applied in several studies of the Baltic Sea (Fennel & Neumann 1996, Neumann et al. 2002, Janssen et al. 2004, Schernewski & Neumann 2005, Neumann & Schernewski 2005, 2008); however, validation of the model did not include validation of the pCO₂ data.

Here, a simple carbon cycle has been included in the model to deal specifically with the pCO₂ at the sea surface. This was accomplished by the addition to the model of the variable C_T , the total CO₂ inorganic carbon (eq. (33)). The equations for C_T are similar to those for other nutrients (phosphate, nitrate etc.). The exchange process at the air-sea border, i.e. the CO₂ flux, is calculated according to

Table 1. State variables of the model

Variable	Meaning	Dimension
O ₂	dissolved oxygen	mmol O ₂ m ⁻³
N		
NH ₄	ammonia	mmol N m ⁻³
NO ₃	nitrate	mmol N m ⁻³
Det _N	nitrogen in detritus	mmol N m ⁻³
Sed _N	nitrogen in sediments	mmol N m ⁻²
P		
PO ₄	phosphate	mmol P m ⁻³
Det _P	phosphate in detritus	mmol P m ⁻³
Sed _P	phosphate in sediments	mmol P m ⁻²
C		
C _T	total CO ₂	mmol C m ⁻³
Det _C	carbon in detritus	mmol C m ⁻³
Sed _C	carbon in sediments	mmol C m ⁻²
Biological parameters		
Dia	diatoms	mmol N m ⁻³
Fla	flagellates	mmol N m ⁻³
Cya _C	carbon in cyanobacteria	mmol C m ⁻³
Cya _N	nitrogen in cyanobacteria	mmol N m ⁻³
Cya _P	phosphate in cyanobacteria	mmol P m ⁻³
Cya _{add}	additional cyanobacteria group	mmol N m ⁻³
Zoo	zooplankton	mmol N m ⁻³

$$C_T^{flux} = k \times k_0 \times (pCO_2 - pCO_2^{atm}), \quad (1)$$

where k is the gas-transfer velocity, k_0 the CO₂ solubility constant, pCO_2 the surface-water CO₂ partial pressure, and pCO_2^{atm} the atmospheric CO₂ partial pressure. The pCO_2^{atm} was described as a function of the Julian day using the seasonality of the CO₂ molar fraction in dry air (Schneider 2011) and taking into account water vapour saturation at the sea surface. pCO_2^{atm} ranges from 365 to 392 μ atm during the year.

The two CO₂ system parameters applied to calculate pCO_2 were total CO₂ C_T and total alkalinity A_T . The CO₂ solubility constant k_0 was calculated according to the method of Weiss (1974). To calculate pCO_2 at the sea surface, the value-iteration method based on the equations of DOE (1994) was used. These calculations entailed the use of thermodynamic equilibrium constants, after Dickson & Millero (1987). The gas-transfer velocity k was calculated according to the method of Liss & Merlivat (1986). C_T was determined from the model (eq. (33)) and A_T was assumed to be constant. For the latter, the mean A_T (1580 μ mol kg⁻¹, as determined by Schneider et al. (2003)) for the eastern Gotland Sea was used. The

assumption of constant alkalinity is justified because calcifying organisms are virtually absent in the central Baltic (Tyrrell et al. 2008) and thus no significant internal changes in A_T occur except the negligible A_T increase by nitrate assimilation. Nevertheless, A_T variations are observed in the central Baltic (see ICES dataset <http://www.ices.dk/ocean>), but these are due to the lateral mixing of water masses which have different background A_T (Hjalmarsson et al. 2008). However, the seasonal changes in pCO₂ are almost independent of the background A_T level. Furthermore, it is not possible to take into account changes in the alkalinity due to the lateral fluxes simply by adjusting it to observations, as at the same time one should adjust C_T and other biochemical parameters, and that would render all the results of a one-dimensional model meaningless. Sensitivity tests of the model with different A_T constant values were performed. The results of these tests showed that a spin-up period of 3 years was enough to adapt the model to various A_T resulting in similar pCO₂ values during the 4th year.

Observations have shown that the elemental composition of cyanobacteria can change dramatically during the growing season. The C:P and N:P ratios of the peak population may exceed the Redfield values (C:N:P = 106:16:1) fourfold, whereas the C:N ratio is near the Redfield ratio (Larsson et al. 2001, Nausch et al. 2004, Degerholm et al. 2006). The increase in the C:P ratio of cyanobacteria (up to 420) strongly influences the carbon cycle. To take into proper account the changes in the elemental composition of cyanobacteria, the model was complemented with variable C:P and N:P ratios for cyanobacteria, detritus and sediment detritus. Thus, the C, N and P components of cyanobacteria, detritus and sediment detritus were treated as independent variables. The derived equations are similar to those in the ‘base’ model (eqs. (17)–(19), (24)–(29)). The parameters of the empirical model for such processes as the mineralization of detritus and sediment detritus, the sedimentation of detritus and cyanobacteria, as well as the mortality of cyanobacteria were assumed to be the same as in the ‘base’ version of the model.

The exception was the cyanobacterial uptake of the nutrients N and C. Thus, in the cyanobacteria equations, the growth term (nitrogen fixation term) was modified and the functions $f_C(\text{PO}_4)$ and $f_N(\text{PO}_4)$ (eqs. (20), (21)) were added to increase the C:P and N:P ratios of cyanobacteria. These functions control the uptake dynamics and increase C:P and N:P ratios in the case of a low PO₄ concentration. The functions were applied in such a way that the modelled C:P and N:P ratios of cyanobacteria matched the maximum according to data from Larsson et al. (2001). This approach was introduced by Kuznetsov et al. (2008).

On the basis of two independent approaches, continuous records of $p\text{CO}_2$ and data for the concentrations of total nitrogen and total phosphorus, Schneider et al. (2009a) provided a possibility for ‘cold fixation’ during spring in the central Baltic Sea. To account for this hypothesis, we added an additional cyanobacteria group, similar to the ‘base’ cyanobacteria group, to the model (eq. (22)). In contrast to the ‘base’ cyanobacteria group, the growth rate of the new cyanobacteria group (Cya_{add}) is not limited by temperature but is strongly phosphate-limited (Table 4, see Appendix page 769). The elemental ratio in this group is constant (Redfield). Cya_{add} reaches maximum abundance in late spring, when the phosphorus concentration is still high. Thus, a dynamic C:N:P ratio for this cyanobacteria group that, as with the ‘base’ cyanobacteria, is dependent on the phosphorous concentration was not included.

The effect of lateral nutrient transport was parameterized as the surface flux. The surface fluxes of nutrients were calibrated in such a way that for the mixed surface layer nutrient concentrations in winter were close to the observations. The constant surface fluxes employed by Burchard et al. (2006) were replaced by time-dependent fluxes (eq. (34)).

The one-dimensional model was applied to a location in the central eastern Gotland Sea with a 240 m water depth (20°E, 57.3°N; see Figure 1). Initial conditions for the variables NO_3 , NH_4 , PO_4 , C_T , O_2 , temperature and salinity were derived from measurements by interpolating observed data. For other variables (Table 1), constant vertical distributions were chosen. Meteorological forcing was available from the European Centre for Medium-Range Weather Forecasts (ECMWF; Persson & Grazzini (2005)). Salinity concentrations were adjusted to observations, with a time scale of $\pi_R = 2$ days. The water column was divided into 240 vertical layers with a resolution of 1 m. The time step for the simulations was $t = 60$ min. The simulations refer to the year 2005 and are discussed together with the $p\text{CO}_2$ measurements from that year.

3. Results and discussion

To assess the effect of the additional cyanobacteria group, Cya_{add} , simulations were performed with a ‘base’ model in which the growth rate for Cya_{add} was set to zero ($r_4^{\max} = 0$, eq. (13)). A spin-up period of three years was applied to adjust the model to initial conditions. Data from the last year of the simulations (January 2005–January 2006) were compared with those measured in 2005. The initial conditions were identical for both simulations. Consequently, the concentrations of some variables differed slightly between the simulations at the beginning of 2005. Furthermore, the surface fluxes of nitrate, ammonia and phosphate were the same for both

simulations, except for the maximum phosphate fluxes during the winter (Table 3, see Appendix page 769).

Because of the difference of primary production parameterization for both simulations, consumption of nutrients differs in time, too: as a result, winter nutrient concentrations differ between the simulations. Winter nutrient concentrations are a major control for production during spring and summer. As the main focus of this study were the surface seasonal changes, the surface nutrient fluxes were parameterized in a such way that winter nutrient concentrations were similar for both simulations. Similar winter phosphate concentrations were obtained by increasing the winter phosphate surface fluxes by about 15%. This value was obtained after preliminary experiments. Changes in phosphate fluxes affected only winter phosphate concentrations in the water column, thus phosphate surface fluxes during spring and summer are similar for both simulations. Such an approach reduced the problem of comparison between simulations. We should also mention that ‘surface fluxes’ in the one-dimensional model represent not only fluxes from atmosphere to water column, but lateral fluxes as well.

Changes in the nutrient and total CO₂ distributions in the below-halocline water by lateral intrusions could not be accounted for by our one-dimensional approach. However, Schneider et al. (2009b) showed that the deep water of the Gotland Sea undergoes a period of stagnation, as they observed from May 2004 to July 2006. Hence, any impact of lateral intrusions on the surface water nutrient and CO₂ budget from deep water was unlikely.

3.1. Average profiles

The means of the 2005 average profiles are compared to statistics from observations in Figure 3. The observation data in Figure 3 are the HELCOM data from the ICES database (<http://www.ices.dk/ocean>). The C_T values shown were recalculated from measured alkalinity, temperature, phosphate, salinity and pH values. The model shows a vertical distribution of all variables resembling observed distributions. The vertical distribution of temperature is well reproduced by the model. As mentioned above, salinity was adjusted to the observations. DIN and DIP were in satisfactory agreement with observations, but at about 50 metres depth DIN concentrations were overestimated. After the formation of the thermal stratification in April to May DIN transport to the surface is limited. At the same time, DIN is rising from the lower layers. DIN has a minimum at around 100 metres depth in the model that can be explained by the oxygen minimum at these depths. Oxygen dynamics were close to the observations, but the depth of the redoxcline was not reproduced by the model quite as well as

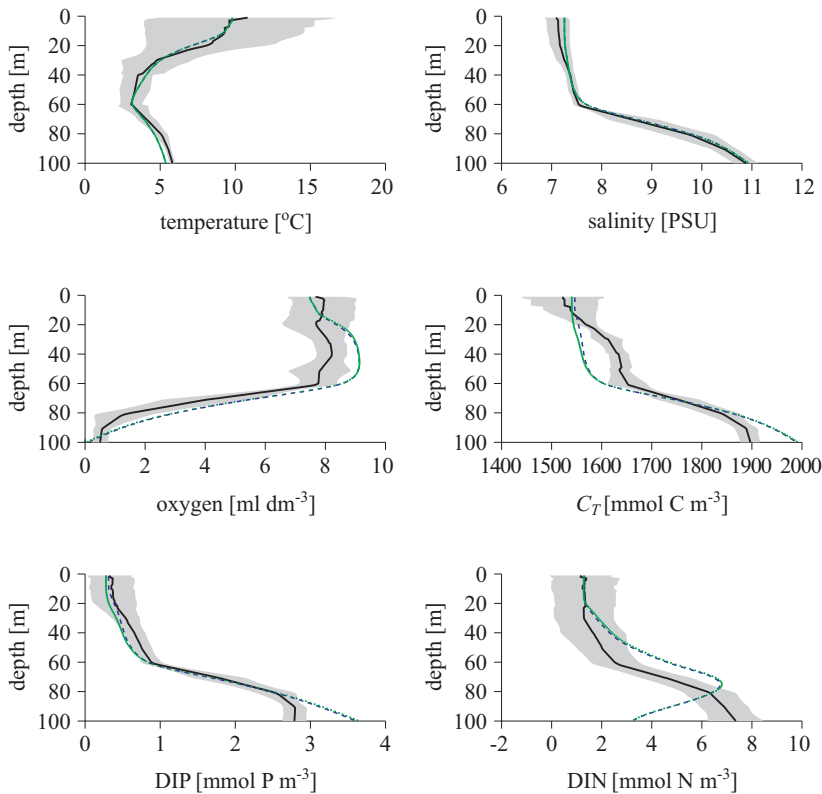


Figure 3. Average (2005) profiles of temperature, salinity, oxygen, total carbon, DIP and DIN. The solid black line and the shaded grey area indicate the mean value and ± 1 standard deviation of the HELCOM data. The dashed blue line indicates the mean of the ‘base’ model, and the green line indicates the mean of the simulation with the additional cyanobacteria group

the local oxygen maximum at ca 50 metres. The dynamics of C_T lie within the range of the observations. Local differences were around a depth of 50 metres where the model showed lower concentrations compared to the observations. At the same time we cannot rule out the errors in observed C_T at around 40 metres owing to the errors in the measurement of pH values.

3.2. Temperature and salinity

Both simulations yielded identical sea surface temperatures (SST) and salinity distributions. SST plays a significant role in the biogeochemical model since it is a controlling factor for flagellate and cyanobacterial growth rates and affects $p\text{CO}_2$ and thus the air/sea CO_2 exchange. Hence, the agreement between modelled and observed SST is crucial to a realistic simulation of the seasonal development of the carbon and nutrient budgets.

Figure 4a indicates that the model reproduced the observed data reasonably well; only during winter was SST slightly underestimated.

3.3. DIN and phosphate

The simulations of the DIN concentrations agreed satisfactorily with the measured data (Figure 4b). Both the DIN increase during winter that is caused by vertical mixing and lateral fluxes, and the complete depletion of DIN at the termination of the spring bloom in March/April were well reproduced. Similarly, phosphate consumption during the spring bloom was simulated reasonably well by the model. However, after the spring bloom, the modelled phosphate concentrations differed from the observed ones and varied between the two simulations. In the simulation with the additional cyanobacteria group, phosphate consumption continued as a result of nitrogen fixation until July, when the concentration approached zero. However, the rate of phosphate consumption in the model was less than the observed rate. In contrast, phosphate concentrations in the 'base' model were approximately constant during May/June because primary production was inhibited for lack of a nitrogen source. A sudden decrease occurred with the onset of the cyanobacterial bloom in mid-June, which led to the complete exhaustion of phosphate in July. In accordance with observations, both nitrate and phosphate concentrations remained close to zero until October/November, when they increased owing to vertical mixing.

3.4. Primary production and pCO₂

During February/March, the surface water was supersaturated with respect to atmospheric CO₂, and as a result of gas exchange pCO₂ decreased slightly (Figure 4e). There were only minor differences between the observed and modelled pCO₂ during this period: these were attributed to a slightly lower model SST. As a consequence of the spring bloom, pCO₂ dropped sharply in March/April, coinciding with the peak in primary production (Figure 4d). The timing of both the onset and the duration of the spring bloom was well reproduced by both simulations. As a result of rising SST and low primary production, the 'base' model generated an increase in pCO₂ after the spring bloom, whereas the measurements showed an almost constant pCO₂ level. The simulations that included production by *Cya_{add}* also resulted in a slight increase in pCO₂, but the deviations from the observations were less significant. The difference between the two simulations was about 100 μatm. However, the discrepancy indicates that the production fuelled by the spring N₂ fixation was slightly underestimated by the model. Cyanobacterial growth started in mid-June and is reflected in both simulations by a sharp drop in pCO₂. This drop was strongest in the

‘base’ model because the entire amount of excess phosphate that remained after the spring bloom was still present in mid-June and led to strong cyanobacterial production (Figure 4d). As a result, the two simulations

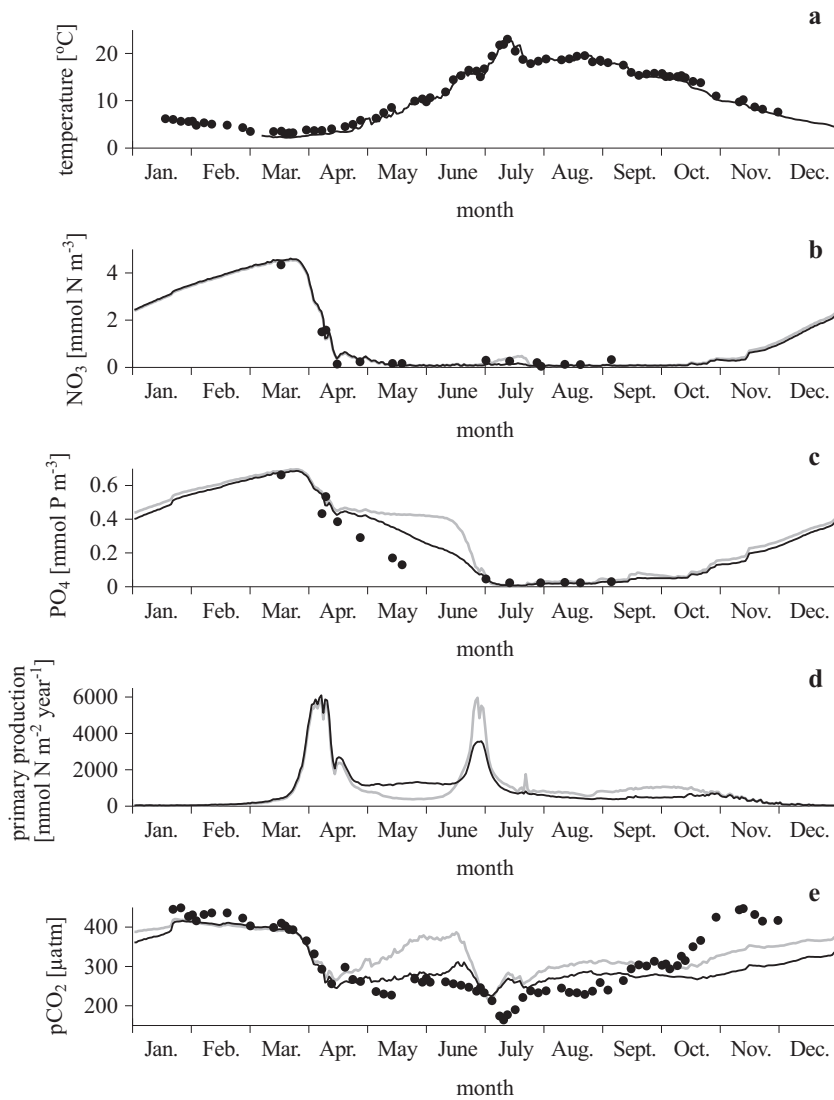


Figure 4. Observations of Schneider et al. (2009a) (black circles) and model results for two simulations (black lines: simulation with additional cyanobacteria group; grey lines: ‘base’ model); a) sea surface temperature, b) dissolved inorganic nitrogen near the sea surface, c) dissolved inorganic phosphate near the sea surface, d) daily averaged primary production, e) CO₂ partial pressure (pCO₂) near the sea surface

yielded almost identical pCO₂ minima in early July, which, however, did not reach the low pCO₂ observed in mid-July. Model runs were also performed with an invariable C:P ratio (106) according to the Redfield hypothesis. In this case, no pCO₂ minimum was obtained and the deviations from the measured data were much larger. After the end of the cyanobacterial bloom, both observations and model simulations showed a sudden increase in pCO₂ that coincided with a decrease in SST (Figure 4a). This increase could be explained by the input of CO₂-enriched deeper water due to vertical mixing. Until October, the measured pCO₂ increased only slightly and was approximately reproduced by the simulations. However, the model was unable to simulate the distinct pCO₂ increase during the deepening of the mixed layer in October. Assuming that the model realistically described the mixing depth, the discrepancy must have resulted from the low CO₂ concentration below the thermocline and thus indicated that the mineralization of organic matter in the simulations was too slow. In the course of the further deepening of the mixed layer until February, the modelled pCO₂ again slowly approached the measured data.

3.5. N₂ fixation rates

Schneider et al. (2009a) used the pCO₂ distribution and data for total nitrogen in the eastern Gotland Sea to estimate N₂ fixation on the basis of mass balances. They hypothesized a spring N₂ fixation that amounted to 74 mmol m⁻², whereas 99 mmol m⁻² was measured for the well-known summer fixation (Table 2). Because of the introduction of *Cya_{add}*, our simulation resulted in almost the same spring N₂ fixation (72 mmol m⁻²). But the model's summer (June/July) N₂ fixation by cyanobacteria (Table 2) exceeded the mass balance estimate by 45% and was beyond the uncertainty range (20%) given by Schneider et al. (2009a). We suspect that the discrepancy was a consequence of different vertical integrations of N₂ fixation. The mass balance was confined to the mixed layer, which had a depth of about 14 m during the cyanobacterial bloom. According to our model, however, the penetration of light controls the

Table 2. Comparison of nitrogen-fixation rates. All values are mmol m⁻² year⁻¹

Time period (Julian day)	Schneider et al. (2009)	Simulation with spring N-fixation	'Base' simulation
April–May	74	71.8	3.3
June–July	99	143.7	174
Total	173	215.5(259)*	177.3(278)*

*Nitrogen-fixation rates calculated for the whole year (January 2005–January 2006).

vertical distribution of N_2 fixation and may stimulate N_2 fixation well below 14 m. As a result, the model yielded an N_2 fixation of 216 mmol m^{-2} for the entire period from April to July, whereas Schneider et al. (2009a) provided an estimate of 173 mmol m^{-2} . In contrast to the mass-balance approach, our simulations also captured N_2 fixation after the onset of mixed-layer deepening, which started in August. The contribution of this late N_2 fixation was 43 mmol m^{-2} resulting in a total annual N_2 fixation of $259 \text{ mmol m}^{-2} \text{ yr}^{-1}$.

In the base simulation, spring N_2 fixation was negligible owing to the absence of Cya_{add} . But since the total phosphate excess was still available in June, N_2 fixation by cyanobacteria was large in June/July and continued more efficiently in the subsequent months. As a result, the total annual N_2 fixation was almost identical in the two simulations.

4. Summary and conclusions

For ecosystem models, pCO_2 is an extremely useful validation variable since it directly reflects the production of organic matter. This is especially important when the nutrient concentrations cannot be used to validate organic matter production because the elemental ratios (C:N, C:P) show large deviations from the Redfield ratios. By incorporating the marine CO_2 system into the model, we have shown that the parameterization of N_2 fixation in the standard ERGOM needs to be modified. We cannot rule out another source for the missing nitrogen. Several model sensitivity tests (extending the model to include dissolved organic matter, different parameterizations of detritus etc.) were done, but they yielded no significant results. By applying a one-dimensional model to the station in the central Gotland Sea we miss all lateral effects. However, such an approach gives us the opportunity to model the main features of the system (like the seasonal variability of the surface nutrients, CO_2 concentrations, primary production, temperature and other important processes for the CO_2 surface cycle) and to elucidate the effect of single processes. In addition, a more detailed representation of the physical processes in the model can improve the dynamics of the biochemical processes. However, only by introducing organisms capable of fixing N_2 during April/May could the model approximately reproduce the observed pCO_2 . Furthermore, the reduction in phosphate immediately after the nitrogen-limited spring bloom was reasonably well simulated by the model. Despite this progress in parameterizing N_2 fixation, we concede that the agreement with the measured pCO_2 and phosphate is not perfect. This indicates that further research on the dynamics and efficiency of N_2 fixation and on the control by phosphorus is necessary.

For the period April–July, the modelled N₂ fixation (216 mmol m⁻²) exceeded the mass-balance estimate (173 mmol m⁻²) of Schneider et al. (2009a). This was attributed to the fact that the model also captured N₂ fixation below the mixed layer. Moreover, the simulations yielded N₂ fixation in August/September, when the mass balance approach could not be applied due to vertical mixing. As a result, the total annual N₂ fixation increased to 259 mmol m⁻² yr⁻¹ and was thus 86 mmol m⁻² yr⁻¹ higher than the value given by Schneider et al. (2009a), which we therefore consider to be a lower-limit estimate.

Acknowledgements

We thank the modelling group of the Leibniz Institute for Baltic Sea Research for providing support for the physical and biogeochemical models. We also thank the reviewers of this paper for their comments, which helped to improve it.

References

- BACC Author Team, 2008, *Annexes*, [in:] *Assessment of climate change for the Baltic Sea Basin*, Springer, New York, 379–398.
- Burchard H., 2002, *Applied turbulence modelling in marine waters*, Lect. Notes Earth Sci., Vol. 100, Springer, Berlin, Heidelberg, New York, 215 pp.
- Burchard H., Bolding K., Kühn W., Meister A., Neumann T., Umlauf L., 2006, *Description of a flexible and extendable physical–biogeochemical model system for the water column*, J. Marine Syst., 61 (3–4), 180–211.
- Degerholm J., Gundersen K., Bergman B., Söderbäck E., 2006, *Phosphorus-limited growth dynamics in two Baltic Sea cyanobacteria, Nodularia sp. and Aphanizomenon sp.*, FEMS Microbiol. Ecol., 58 (3), 323–332, doi:10.1111/j.1574-6941.2006.00180.x.
- Dickson A., Millero F. J., 1987, *A comparison of the equilibrium constants for the dissociation of carbonic acid in seawater media*, Deep-Sea Res., 34 (10), 1733–1743, doi:10.1016/0198-0149(87)90021-5.
- DOE, 1994, *Handbook of methods for the analysis of the various parameters of the carbon dioxide system in sea water; version 2.0*, A. G. Dickson & C. Goyet (eds.), ORNL/CDIAC-74.
- Fennel W., Neumann T., 1996, *The mesoscale variability of nutrients and plankton as seen in a coupled model*, Ger. J. Hydrogr., 48 (1), 49–71, doi:10.1007/BF02794052.
- HELCOM, 2003, *The Baltic marine environment 1999–2002*, Baltic Sea Environ. Proc., 87, 47 pp.
- Hjalmarsson S., Wesslander K., Anderson L. G., Omstedt A., Perttilä M., Mintrop L., 2008, *Distribution, long-term development and mass balance calculation*

- of total alkalinity in the baltic sea*, Cont. Shelf Res., 28(4–5), 593–601, doi:10.1016/j.csr.2007.11.010.
- Howarth R., Marino R., Lane J., Cole J., 1988, *Nitrogen fixation in freshwater, estuarine, and marine ecosystems. 1. Biogeochemical controls*, Limnol. Oceanogr., 33(4 pt. 2), 669–687, doi:10.4319/lo.1988.33.4.part.2.0669.
- ICES, 2009, *ICES dataset on ocean hydrography*, The International Council for the Exploration of the Sea, Copenhagen.
- Janssen F., Neumann T., Schmidt M., 2004, *Inter-annual variability in cyanobacteria blooms in the Baltic Sea controlled by wintertime hydrographic conditions*, Mar. Ecol.-Prog. Ser., 275, 59–68, doi:10.3354/meps275059.
- Kahru M., Savchuk O., Elmgren R., 2007, *Satellite measurements of cyanobacterial bloom frequency in the Baltic Sea: interannual and spatial variability*, Mar. Ecol.-Prog. Ser., 343, 15–23, doi:10.3354/meps06943.
- Kuznetsov I., Neumann T., Burchard H., 2008, *Model study on the ecosystem impact of a variable C:N:P ratio for cyanobacteria in the Baltic Proper*, Ecol. Model., 219(1–2), 107–114, doi:10.1016/j.ecolmodel.2008.08.002.
- Larsson U., Hajdu S., Walve J., Elgrem R., 2001, *Baltic Sea nitrogen fixation estimated from the summer increase in upper mixed layer total nitrogen*, Limnol. Oceanogr., 46(4), 811–820, doi:10.4319/lo.2001.46.4.0811.
- Leinweber A., 2002, *Saisonal Kohlenstoffkreislauf im Oberflächenwasser der zentralen Ostsee: numerische Prozessstudien zur Simulation des CO₂-Partialdrucks*, Ph.D. thesis, Rostock Univ.
- Liss P., Merlivat L., 1986, *Air-sea gas exchange rates: introduction and synthesis*, [in:] *The role of air-sea exchange in geochemical cycling*, P. Buat-Ménard, NATO ASI Ser., Vol. 185, Reidel, Dordrecht, 113–127.
- Muller-Navarra D.C., Brett M.T., Liston A.M., Goldman C.R., 2000, *A highly unsaturated fatty acid carbon transfer between primary producers and consumers*, Nature, 403(6765), 74–76, 10.1038/47469.
- Nausch M., Nausch G., Wasmund N., 2004, *Phosphorus dynamics during the transition from nitrogen to phosphate limitation in the central Baltic Sea*, Mar. Ecol.-Prog. Ser., 266, 15–25, doi:10.3354/meps266015.
- Neumann T., Fennel W., Kremp C., 2002, *Experimental simulations with an ecosystem model of the Baltic Sea: A nutrient load reduction experiment*, Global Biogeochem. Cy., 16(3), 450, doi:10.1029/2001GB001450.
- Neumann T., Schernewski G., 2005, *An ecological model evaluation of two nutrient abatement strategies for the Baltic Sea*, J. Marine Syst., 56(1–2), 195–206, doi:10.1016/j.jmarsys.2004.10.002.
- Neumann T., Schernewski G., 2008, *Eutrophication in the Baltic Sea and shifts in nitrogen fixation analyzed with a 3D ecosystem model*, J. Marine Syst., 74(1–2), 592–602, doi:10.1016/j.jmarsys.2008.05.003.
- Omstedt A., Gustafsson E., Wesslander K., 2009, *Modelling the uptake and release of carbon dioxide in the Baltic Sea surface water*, Cont. Shelf Res., 29(7), 870–885, doi:10.1016/j.csr.2009.01.006.

- Persson A., Grazzini F., 2005, *User guide to ECMWF forecast products*, Meteorol. Bull., M3.2, 153 pp.
- Rahm L., Jonsson A., Wulff F., 2000, *Nitrogen fixation in the Baltic Proper: an empirical study*, J. Marine Syst., 25 (3–4), 239–248, doi:10.1016/S0924-7963(00)00018-X.
- Savchuk O., Wulff F., 1999, *Modelling regional and large-scale response of Baltic Sea ecosystems to nutrient load reductions*, Hydrobiologia, 393 (0), 35–43, doi:10.1023/A:1003529531198.
- Schernewski G., Neumann T., 2005, *The trophic state of the Baltic Sea a century ago: a model simulation study*, J. Marine Syst., 53 (1–4), 109–124, doi:10.1016/j.jmarsys.2004.03.007.
- Schneider B., 2011, *The CO₂ system of the Baltic Sea: Biogeochemical control and impact of anthropogenic CO₂*, [in:] *Global change and baltic coastal zones*, G. Schernewski, J. Hofstede & T. Neumann (eds.), Coastal Res. Lib., Vol. 1, Springer, Dordrecht, 33–50.
- Schneider B., Kaitala S., Maunula P., 2006, *Identification and quantification of plankton bloom events in the Baltic Sea by continuous pCO₂ and chlorophyll a measurements on a cargo ship*, J. Marine Syst., 59 (3–4), 238–248, doi:10.1016/j.jmarsys.2005.11.003.
- Schneider B., Kaitala S., Raateoja M., Sadkowiak B., 2009a, *A nitrogen fixation estimate for the Baltic Sea based on continuous pCO₂ measurements on a cargo ship and total nitrogen data*, Cont. Shelf Res., 29 (11–12), 1535–1540, doi:10.1016/j.csr.2009.04.001.
- Schneider B., Nausch G., Nagel K., Wasmund N., 2003, *The surface water CO₂ budget for the Baltic Proper: a new way to determine nitrogen fixation*, J. Marine Syst., 42 (1–2), 53–64, doi:10.1016/S0924-7963(03)00064-2.
- Schneider B., Nausch G., Pohl C., 2009b, *Mineralization of organic matter and nitrogen transformations in the Gotland Sea deep water*, Deep-Sea Res., (in press).
- Stigebrandt A., Wulff F., 1987, *A model for the dynamics of nutrients and oxygen in the Baltic Proper*, J. Mar. Res., 45 (3), 729–759, doi:10.1357/002224087788326812.
- Tyrrell T., Schneider B., Charalampopoulou A., Riebesell U., 2008, *Coccolithophores and calcite saturation state in the Baltic and Black Seas*, Biogeosciences, 5 (2), 485–494, doi:10.5194/bg-5-485-2008.
- Umlauf L., Burchard H., 2003, *A generic length-scale equation for geophysical turbulence models*, J. Mar. Res., 61 (2), 235–265, doi:10.1357/002224003322005087.
- Umlauf L., Burchard H., 2005, *Second-order turbulence closure models for geophysical boundary layers. A review of recent work*, Cont. Shelf Res., 25 (7–8), 795–827, doi:10.1016/j.csr.2004.08.004.
- Wasmund N., 1997, *Occurrence of cyanobacterial blooms in the Baltic Sea in relation to environmental conditions*, Int. Rev. Ges. Hydrobio., 82 (2), 169–184, doi:10.1002/iroh.19970820205.

- Wasmund N., Voss M., Lochte K., 2001, *Evidence of nitrogen fixation by non-heterocystous cyanobacteria in the Baltic Sea and re-calculation of a budget of nitrogen fixation*, Mar. Ecol.-Prog. Ser., 214, 1–14, doi:10.3354/meps214001.
- Weiss R., 1974, *Carbon dioxide in water and seawater: the solubility of a non-ideal gas*, Mar. Chem., 2 (3), 203–215, doi:10.1016/0304-4203(74)90015-2.

Appendix

Biogeochemical model equations and parameters

The model described here in detail consists of 18 state variables (see Table 1). The general structure of a one-dimensional biogeochemical model expressed as ensemble-averaged concentrations is given by the following set of equations:

$$\begin{aligned} \partial_t c_i + \partial_z(m_i c_i - K_V \partial_z c_i) &= R_{c_i}, \\ i &= 1, \dots, 18, \end{aligned} \quad (2)$$

where $\vec{c} = (c_1, \dots, c_{18})^T$ denotes the concentrations of the state variables, m_i the autonomous motion of the ecosystem component m_i (e.g. sinking or active swimming) and K_V the eddy diffusivity (Burchard et al. 2006). The source and sink terms of the ecosystem component c_i are summarized as R_{c_i} .

The biogeochemical model described in this study is based on the ERGOM Baltic Sea ecosystem model (Neumann et al. 2002). The present model simulates the C, N, and P components of cyanobacteria, detritus and sediment detritus separately. The stoichiometries of all phytoplankton groups (except the 'base' cyanobacteria) and zooplankton are fixed at the Redfield ratio (C:N:P = 106:16:1). The basic structure of the model is explained in Figure 2. Constants and parameters not cited in the text are presented in Tables 3–7.

Two different limiting functions proposed by Burchard et al. 2006 are used. Heavyside switches, as in Neumann et al. (2002), are converted to a smoothed hyperbolic tangent transition with prescribed width x_w :

$$\theta(x, x_w, y_{\min}, y_{\max}) = y_{\min} + (y_{\max} - y_{\min}) \frac{1}{2} \left(1 - \tanh \left(\frac{x}{x_w} \right) \right). \quad (3)$$

Also, as a limiting function, a modified Michaelis-Menten formula with squared arguments, as stated by Fennel & Neumann (1996) is used:

$$Y(x_w, x) = \frac{x^2}{x_w^2 + x^2}. \quad (4)$$

Similarly to Burchard et al. (2006), the limits constructed by eqs. (3) and (4) are used for chemical reactions that depend on the availability of oxygen and nitrate:

$$\begin{aligned} l_+^+ &= \theta(\text{O}_2, \text{O}_2^t, 0, 1) Y(\text{NO}_3^t, \text{NO}_3), \\ l_+^- &= \theta(-\text{O}_2, \text{O}_2^t, 0, 1) Y(\text{NO}_3^t, \text{NO}_3), \\ l_-^- &= \theta(-\text{O}_2, \text{O}_2^t, 0, 1) (1 - Y(\text{NO}_3^t, \text{NO}_3)), \end{aligned} \quad (5)$$

$$L_+^+ = \frac{l_+^+}{l_+^+ + l_+^- + l_-^-},$$

$$L_+^- = \frac{l_+^-}{l_+^+ + l_+^- + l_-^-},$$

$$L_-^- = \frac{l_-^-}{l_+^+ + l_+^- + l_-^-}.$$

For phytoplankton, the light-limitation function PPI as well as other rates are assumed to be the same for all phytoplankton groups:

$$PPI = \frac{I_{par}}{I_{opt}} \exp\left(1 - \frac{I_{par}}{I_{opt}}\right), \quad (6)$$

where I_{opt} , the optimum irradiance for algal photosynthesis, is

$$I_{opt} = \max\left(\frac{I_0}{4}, I_{min}\right) \quad (7)$$

and I_0 is the albedo-corrected surface radiation. The photosynthetically available radiation I_{PAR} follows from

$$I_{PAR}(z) = I_0(1 - a) \exp\left(\frac{z}{\eta_2}\right) B(z), \quad (8)$$

where $B(z)$ denotes absorption of the blue-green part of the light spectrum by phytoplankton and detritus:

$$B(z) = \exp\left(-k_c \int_z^0 (P_{sum}(\xi) + Det_N(\xi)) d\xi\right). \quad (9)$$

The variables in eqs. (8) and (9) are the absorption-length scales for the blue-green part of the light spectrum η_2 , the weighting parameter a and the attenuation constant for self-shading k_c . The coordinate z is taken to point upwards with the origin $z = 0$ at the mean sea surface elevation. $P_{sum} = Dia + Fla + Cya_N + Cya_{add}$ is the sum of the concentrations of all phytoplankton groups as expressed in nitrogen units.

Since the diatom *Dia* bloom is in early spring, when the temperature is low, the growth rate for diatoms is independent of temperature:

$$R_1 = r_1^{\max} \min[Y(\alpha_1, \text{NH}_4 + \text{NO}_3), Y(s_{NP}\alpha_1, \text{PO}_4), PPI]. \quad (10)$$

Flagellates *Fla*, in contrast to diatoms, reach their highest abundances in summer and benefit from moderate temperatures (Neumann et al. 2002):

$$R_2 = r_2^{\max} (1 + Y(T_f, T)), \quad (11)$$

$$\min[Y(\alpha_2, \text{NH}_4 + \text{NO}_3), Y(s_{NP}\alpha_2, \text{PO}_4), PPI].$$

Like the growth rate of flagellates, that of cyanobacteria depends on temperature, but, unlike flagellates and diatoms, cyanobacteria are not limited by nitrate:

$$R_3 = r_3^{\max} \frac{1}{1 + \exp(\beta_{bg}(T_{bg} - T))} \min[Y(s_{NP}\alpha_3, \text{PO}_4), PPI]. \quad (12)$$

The expression for the cyanobacterial growth rate is based on observations (see Wasmund 1997). The growth rate for the additional cyanobacteria group is parameterized in the same way as for the 'base' cyanobacteria, except that the temperature dependence is dropped. Also, the half-saturation constant has been increased.

$$R_4 = r_4^{\max} \min[Y(s_{NP}\alpha_4, \text{PO}_4), PPI]. \quad (13)$$

In addition, compared to the original ERGOM model of Neumann et al. (2002), the maximum growth rates as well as the half-saturation and temperature-control constants have been changed due to the fact that ERGOM, as developed by Neumann et al. (2002), is a three-dimensional version for the entire Baltic Sea, such that all phytoplankton constants are applied to all regions of the Baltic Sea. By contrast, the present one-dimensional model is applied only to the Gotland Sea.

Grazing by zooplankton depends on the temperature and is less efficient for the ingestion of cyanobacteria (see, e.g., Muller-Navarra et al. 2000),

$$G_n = g_n^{\max} \left(1 + \frac{T^2}{T_{opt}^2} \exp\left(1 - \frac{2T}{T_{opt}}\right) \right) (1 - \exp(-I_{Ivlev} P_{sum}^2)), \quad (14)$$

where g_n^{\max} are maximum grazing rates, T_{opt} is the optimum temperature and I_{Ivlev} a modified Ivlev constant (Neumann et al. 2002).

Diatoms of the phytoplankton group evolve in accordance with:

$$\frac{d}{dt} Dia = R_1 Dia - l_{PA} Dia - l_{PD} Dia - G_1 \frac{Dia}{P_{sum}} Zoo. \quad (15)$$

The equation for the flagellates is:

$$\frac{d}{dt} Fla = R_2 Fla - l_{PA} Fla - l_{PD} Fla - G_2 \frac{Fla}{P_{sum}} Zoo. \quad (16)$$

Diatoms and flagellates can be characterized by the Redfield ratio, whereas cyanobacteria can be represented by ratios other than the Redfield one. For cyanobacteria, there are three state variables, one for each compound (C, N, and P):

$$\frac{d}{dt} Cya_C = f_C(\text{PO}_4) R_3 Cya_C - l_{PA} Cya_C - l_{PD} Cya_C - G_3 \frac{Cya_C}{P_{sum}} Zoo, \quad (17)$$

$$\frac{d}{dt} Cya_N = f_N(\text{PO}_4) R_3 Cya_N - l_{PA} Cya_N - l_{PD} Cya_N - G_3 \frac{Cya_N}{P_{sum}} Zoo, \quad (18)$$

$$\frac{d}{dt}Cya_P = R_3Cya_P - l_{PA}Cya_P - l_{PD}Cya_P - G_3\frac{Cya_P}{P_{sum}}Z_{oo}. \quad (19)$$

The modified model includes a dynamic C:N:P = (106–400):(16–60):1 ratio for cyanobacteria with the relation:

$$f_C(\text{PO}_4) = 106 + 147 \left(1 + \tanh \left(\frac{\gamma_{P0} - \text{PO}_4}{\gamma_{P1}} \right) \right), \quad (20)$$

$$f_N(\text{PO}_4) = 16 + 22 \left(1 + \tanh \left(\frac{\gamma_{P0} - \text{PO}_4}{\gamma_{P1}} \right) \right), \quad (21)$$

$\gamma_{P0} = 0.1$ [mmol P m⁻³] is a constant that defines the phosphate concentration, in which the changes in the cyanobacteria C:P and N:P ratios double; $\gamma_{P1} = 0.03$ [mmol P m⁻³] is a constant that determines the rate of change of C:P and N:P ratios. $f_C(\text{PO}_4)$ ranges from 106 to 400, and $f_N(\text{PO}_4)$ from 16 to 60.

The additional cyanobacteria group Cya_{add} is included in the Redfield ratio. Cya_{add} , in contrast to the ‘base’ cyanobacteria, reaches maximum abundances in late spring, while the phosphate concentration is still high; hence, including a dynamic C:N:P ratio for this cyanobacteria group that depends on phosphate concentration as is the case for the ‘base’ cyanobacteria is not reasonable.

$$\frac{d}{dt}Cya_{add} = R_4Cya_{add} - l_{PA}Cya_{add} - l_{DP}Cya_{add} - G_4\frac{Cya_{add}}{P_{sum}}Z_{oo}. \quad (22)$$

The model zooplankton evolve according to:

$$\frac{d}{dt}Z = \frac{G_1Dia + G_2Fla + G_3Cya_N + G_4Cya_{add}}{P_{sum}}Z - l_{ZA}Z^2 - l_{ZD}Z^2, \quad (23)$$

where l_{ZA} and l_{ZD} are constant rates for the mortality and excretion of zooplankton respectively. Ratios between the terms $-G_3\frac{Cya_C}{P_{sum}}Z_{oo}$: $-G_3\frac{Cya_N}{P_{sum}}Z_{oo}$: $-G_3\frac{Cya_P}{P_{sum}}Z_{oo}$ in eqs. (17)–(19) may be outside the Redfield ratio. However, the model zooplankton remain at the Redfield ratio, but grazing on phytoplankton is outside it. To solve these problems with an additional sink for C and N, additional source terms in the detritus equations have been assumed; thus, the system is completed as follows: $+G_3\frac{Cya_C - 106Cya_P}{P_{sum}}Z_{oo}$ in the equation for Det_C (eq. (24)) and $+G_3\frac{Cya_N - 16Cya_P}{P_{sum}}Z_{oo}$ in the equation for Det_N (eq. (24)). This means that parts of the N and C components are transferred to the detritus immediately. The detritus variable, as in Neumann et al. (2002), is divided into three state variables for each compound, C, N, and P. The detritus equations are then:

$$\begin{aligned} \frac{d}{dt} Det_C = l_{PD} (s_{NC} (Dia + Fla + Cya_{add}) + Cya_C) + s_{NC} l_{ZD} Zoo^2 + \quad (24) \\ + G_3 \frac{Cya_C - 106Cya_P}{P_{sum}} Zoo - L_{DA} Det_C - l_{DS} \frac{Det_C}{H_{bottom}} \delta_{k,k_{bottom}}, \end{aligned}$$

$$\begin{aligned} \frac{d}{dt} Det_N = l_{PD} (Dia + Fla + Cya_{add} + Cya_N) + l_{ZD} Zoo^2 + \quad (25) \\ + G_3 \frac{Cya_N - 16Cya_P}{P_{sum}} Zoo - L_{DA} Det_N - l_{DS} \frac{Det_N}{H_{bottom}} \delta_{k,k_{bottom}}, \end{aligned}$$

$$\begin{aligned} \frac{d}{dt} Det_P = l_{PD} (s_{NP} (Dia + Fla + Cya_{add}) + Cya_P) + s_{NP} l_{ZD} Zoo^2 + \quad (26) \\ - L_{DA} Det_P - l_{DS} \frac{Det_P}{H_{bottom}} \delta_{k,k_{bottom}}, \end{aligned}$$

where $L_{DA} = l_{DA}(1 + \beta_{DAY}(T_{DA}, T))$ is the temperature dependent mineralization of detritus, l_{DS} the sedimentation rate, H_{bottom} the thickness of the box next to the bottom, and $\delta_{k,k_{bottom}}$ the Kronecker delta, indicating that this term exists only in the bottom layer of the model with index $k = k_{bottom}$. As with detritus, sediment detritus is described by three state variables, one for each compound, C, N, and P:

$$\frac{d}{dt} Sed_C = l_{DS} Det_C \delta_{k,k_{bottom}} - L_{SA} Sed_C, \quad (27)$$

$$\frac{d}{dt} Sed_N = l_{DS} Det_N \delta_{k,k_{bottom}} - L_{SA} Sed_N, \quad (28)$$

$$\frac{d}{dt} Sed_P = l_{DS} Det_P \delta_{k,k_{bottom}} - L_{SA} Sed_P, \quad (29)$$

where $L_{SA} = l_{SA} \exp(\beta_{SAT}) \theta(O_2, O_2^t, 0.2, 2)$ is the sediment mineralization rate under oxic and anoxic conditions. The state equations for nitrate, ammonium, phosphate and total carbon dynamics lead to:

$$\frac{d}{dt} NH_4 = - \frac{NH_4}{NH_4 + NO_3} (R_1 Dia + R_2 Fla) + l_{PA} P_{sum} + \quad (30)$$

$$+ l_{ZA} Z^2 + L_{DA} Det_N - L_{AN} NH_4 + \frac{NH_4^{flux}}{H_{surf}} \delta_{k,k_{surf}} +$$

$$+ \theta(O_2, O_2^t, 0.5, 1) L_{SA} \frac{Sed_N}{H_{bottom}} \delta_{k,k_{bottom}},$$

$$\frac{d}{dt} NO_3 = - \frac{NO_3}{NH_4 + NO_3} (R_1 Dia + R_2 Fla) + L_{AN} NO_3 + \quad (31)$$

$$\begin{aligned}
& + \frac{\text{NO}_3^{\text{flux}}}{H_{\text{surf}}} \delta_{k,k_{\text{surf}}} - s_{ND} \left(L_{DA} \text{Det}_C + L_{SA} \frac{\text{Sed}_C}{H_{\text{bottom}}} \delta_{k,k_{\text{bottom}}} \right) L_+^-, \\
\frac{d}{dt} \text{PO}_4 & = s_{NP} [-R_1 \text{Dia} - R_2 \text{Fla} - R_4 \text{Cya}_{\text{add}} + \\
& + l_{PA} (\text{Dia} + \text{Fla} + \text{Cya}_{\text{add}}) + l_{ZA} Z^2] + \\
& - R_4 \text{Cya}_P + l_{PA} \text{Cya}_P + L_{DA} \text{Det}_P + \frac{\text{PO}_4^{\text{flux}}}{H_{\text{surf}}} \delta_{k,k_{\text{surf}}} + \\
& + L_{SA} \left(1 - p_1 \theta(\text{O}_2, \text{O}_2^t, 0, 1) Y(p_2, \text{O}_2) \right) \frac{\text{Sed}_P}{H_{\text{bottom}}} \delta_{k,k_{\text{bottom}}},
\end{aligned} \tag{32}$$

$$\begin{aligned}
\frac{d}{dt} C_T & = s_{NC} [-R_1 \text{Dia} - R_2 \text{Fla} - R_4 \text{Cya}_{\text{add}} + \\
& + l_{PA} (\text{Dia} + \text{Fla} + \text{Cya}_{\text{add}}) + l_{ZA} Z^2] + \\
& - R_4 \text{Cya}_C + l_{PA} \text{Cya}_C + L_{DA} \text{Det}_C + \\
& + L_{SA} \frac{\text{Sed}_C}{H_{\text{bottom}}} \delta_{k,k_{\text{bottom}}} + \frac{C_T^{\text{flux}}}{H_{\text{surf}}} \delta_{k,k_{\text{surf}}}.
\end{aligned} \tag{33}$$

The nutrient uptake of diatoms and flagellates involves a preference for ammonium by means of the ratios $\frac{A}{A+N}$ and $\frac{N}{A+N}$. Nutrient fluxes on the upper boundary have been added as source terms in the nutrient equations with the Kronecker delta $\delta_{k,k_{\text{surf}}}$. $L_{AN} = l_{AN} \theta(\text{O}_2, \text{O}_2^t, 0, 1) \frac{\text{O}_2}{\text{O}_{AN} + \text{O}_2} \exp(\beta_{ANT})$ is the nitrification rate which is controlled by oxygen and temperature (Stigebrandt & Wulff 1987). The last term in eq. (31) is the response to denitrification. The nutrient surface fluxes are prescribed by

$$\begin{aligned}
c_i^{\text{flux}} & = \theta(\text{day} - 330, \delta_{\text{day}}, c_i^{\text{flux}}_{\text{min}}, c_i^{\text{flux}}_{\text{max}}) + \\
& + \theta(100 - \text{day}, \delta_{\text{day}}, c_i^{\text{flux}}_{\text{min}}, c_i^{\text{flux}}_{\text{max}})
\end{aligned} \tag{34}$$

with $\vec{c}^{\text{flux}} = (\text{NH}_4^{\text{flux}}, \text{NO}_3^{\text{flux}}, \text{PO}_4^{\text{flux}})$ denoting the surface fluxes of nutrients. day represents day of the year, $c_i^{\text{flux}}_{\text{min}}$ is the minimum (summer) flux values, and $c_i^{\text{flux}}_{\text{max}}$ the maximum (winter) values of the fluxes (see Table 3). $\delta_{\text{day}} = 15$ [day] is a constant that defines the half-value of the time during which changes in fluxes from $c_i^{\text{flux}}_{\text{min}}$ to $c_i^{\text{flux}}_{\text{max}}$ occur. θ is a smoothed hyperbolic tangent transition of prescribed width (eq. (3)). Thus, the effect of winter lateral nutrient transport and atmospheric nutrients deposition has been taken into account.

The oxygen dynamics are described by

$$\begin{aligned} \frac{d}{dt}O_2 = & \frac{s_{NC}NH_4 + s_{NO}NO_3}{NH_4 + NO_3} (R_1Dia + R_2Fla) + R_3Cya_C + \quad (35) \\ & + s_{NC}R_4Cya_{add} + s_{NC}l_{ZA}Z^2 - s_{ON}L_{AN}NH_3 + \\ & - l_{PA}(s_{NC}(Dia + Fla + Cya_{add}) + Cya_C) + \\ & - \left(L_+^+ + L_-^-\right) \left(L_{DA}Det_C + L_{SA} \frac{Sed_C}{H_{bottom}} \delta_{k,k_{bottom}}\right) + \\ & - \theta(O_2, O_2^t, 0, 0.5)L_{SA} \frac{Sed_N}{H_{bottom}} \delta_{k,k_{bottom}} + \frac{O_2^{flux}}{H_{surf}} \delta_{k,k_{surf}}. \end{aligned}$$

Oxygen is consumed through respiration, nitrification and mineralization. The sources for oxygen are primary production and fluxes at the upper boundary. The surface flux is prescribed by

$$O_2^{flux} = p_{vel} (O_{sat} - O_2), \quad (36)$$

where

$$O_{sat} = a_0 (a_1 + a_2 T) \quad (37)$$

with $a_0 = 31.25 \text{ mmol m}^{-3}$, $a_1 = 14.603$, and $a_2 = 0.4025 \text{ T}^{-1}$ (Neumann et al. 2002).

Table 3. The surface fluxes of nutrients

c_i^{flux}	$c_i^{flux}_{min}$	$c_i^{flux}_{max}$	Dimension
NH_4^{flux}	0.05	0.4	[mmol N m ² d ⁻¹]
NO_3^{flux}	0.1	0.7	[mmol N m ² d ⁻¹]
PO_4^{flux}	0.01	0.14 ^(a) 0.12 ^(b)	[mmol P m ² d ⁻¹]

^(a)for the simulation with an additional cyanobacteria group.

^(b)for the ‘base’ model.

Table 4. Phytoplankton rates

Parameters	<i>Dia</i>	<i>Fla</i>	<i>Cya_X</i>	<i>Cya_{add}</i>
growth rate	$r_1^{\max} = 1.35 \text{ d}^{-1}$	$r_2^{\max} = 0.6 \text{ d}^{-1}$	$r_3^{\max} = 0.85 \text{ d}^{-1}$	$r_4^{\max} = 1.3 \text{ d}^{-1}$
half-saturation	$\alpha_1 = 1.35$	$\alpha_2 = 0.2$	$\alpha_3 = 0.75$	$\alpha_4 = 12$
sinking speed	$m_1 = -50 \text{ cm d}^{-1}$	$m_2 = 0 \text{ cm d}^{-1}$	$m_3 = 10 \text{ cm d}^{-1}$	$m_4 = 0 \text{ cm d}^{-1}$
respiration	$l_{PA} = 0.01 \text{ d}^{-1}$	$l_{PA} = 0.01 \text{ d}^{-1}$	$l_{PA} = 0.01 \text{ d}^{-1}$	$l_{PA} = 0.01 \text{ d}^{-1}$
mortality	$l_{PD} = 0.05 \text{ d}^{-1}$	$l_{PD} = 0.05 \text{ d}^{-1}$	$l_{PD} = 0.05 \text{ d}^{-1}$	$l_{PD} = 0.05 \text{ d}^{-1}$
temperature control	-	$T_f = 10^\circ\text{C}$	$T_{bg} = 13^\circ\text{C}$ $\beta_{bg} = 0.1^\circ\text{C}^{-1}$	-

Table 5. Biogeochemical process rates

Parameter	Notation and value
<i>Nitrification</i>	
nitrification constant	$l_{AN} = 0.1 \text{ d}^{-1}$
oxygen parameter	$O_{AN} = 0.01$
temperature control	$\beta_{AN} = 0.11 \text{ }^{\circ}\text{C}^{-1}$
<i>Mineralization</i>	
detritus mineralization constant	$l_{DA} = 0.003 \text{ d}^{-1}$
temperature control	$T_{DA} = 13 \text{ }^{\circ}\text{C}, \beta_{DA} = 20$
sediment mineralization constant	$l_{SA} = 0.001 \text{ d}^{-1}$
temperature control	$\beta_{SA} = 0.15 \text{ }^{\circ}\text{C}^{-1}$
release of phosphate	$p_1 = 0.15, p_2 = 0.1$
oxygen tolerance	$O_2^t = 60 \text{ mmol O}_2 \text{ m}^{-3}$
nitrate tolerance	$\text{NO}_3^t = 0.1 \text{ mmol N m}^{-3}$

Table 6. Zooplankton rates

Parameter	Notation	Value
grazing on <i>Dia</i>	g_1^{\max}	$1 : \text{d}^{-1}$
grazing on <i>Fla</i>	g_2^{\max}	$1 : \text{d}^{-1}$
grazing on <i>Cya_X</i>	g_3^{\max}	$0.7 : \text{d}^{-1}$
grazing on <i>Cya_{add}</i>	g_4^{\max}	$0.7 : \text{d}^{-1}$
exudation	l_{ZA}	$0.06 \text{ mmol N d}^{-1} \text{ m}^{-3}$
mortality	l_{ZD}	$0.13 \text{ mmol N d}^{-1} \text{ m}^{-3}$
Ivlev constant	I_{Ivlev}	0.24
optimum temperature	T_{opt}	20°C

Table 7. Other parameters

minimum irradiance	$I_{\min} = 25 \text{ Wm}^{-2}$
detritus sinking	$m_{\text{det}} = 3 \text{ m d}^{-1}$
sedimentation rate	$l_{DS} = 3.5 \text{ m d}^{-1}$
piston velocity	$p_{\text{vel}} = 5 \text{ m d}^{-1}$
Redfield ratio (P:N)	$s_{NP} = 0.0625$
Redfield ratio (C:N)	$s_{NC} = 6.625$
oxygen production related to N	$s_{NO} = 8.625$
nitrification constant	$s_{ON} = 2$
reduced nitrate/oxidized detritus	$s_{ND} = 0.8$